

# New results for light gravitinos at hadron colliders: Fermilab Tevatron limits and CERN LHC perspectives

Michael Klasen\*

*Institut für Theoretische Physik, Universität Göttingen, Friedrich-Hund-Platz 1, D-37077 Göttingen, Germany  
and Laboratoire de Physique Subatomique et de Cosmologie, Université Joseph Fourier/CNRS-IN2P3,  
53 Avenue des Martyrs, F-38026 Grenoble, France*

Guillaume Pignol

*Laboratoire de Physique Subatomique et de Cosmologie, Université Joseph Fourier/CNRS-IN2P3,  
53 Avenue des Martyrs, F-38026 Grenoble, France*

(Received 13 October 2006; revised manuscript received 13 April 2007; published 4 June 2007)

We derive Feynman rules for the interactions of a single gravitino with (s)quarks and gluons/gluinos from an effective supergravity Lagrangian in nonderivative form and use them to calculate the hadro-production cross sections and decay widths of single gravitinos. We confirm the results obtained previously with a derivative Lagrangian as well as those obtained with the nonderivative Lagrangian in the high-energy limit and elaborate on the connection between gauge independence and the presence of quartic vertices. We perform extensive numerical studies of branching ratios, total cross sections, and transverse-momentum spectra at the Fermilab Tevatron and the CERN LHC. From the latest CDF monojet cross section limit, we derive a new and robust exclusion contour in the gravitino-squark/gluino mass plane, implying that gravitinos with masses below  $2 \times 10^{-5}$  to  $1 \times 10^{-5}$  eV are excluded for squark/gluino masses below 200 and 500 GeV, respectively. These limits are complementary to the one obtained by the CDF Collaboration,  $1.1 \times 10^{-5}$  eV, under the assumption of infinitely heavy squarks and gluinos. For the LHC, we conclude that supersymmetric scenarios with light gravitinos will lead to a striking monojet signal very quickly after its startup.

DOI: [10.1103/PhysRevD.75.115003](https://doi.org/10.1103/PhysRevD.75.115003)

PACS numbers: 12.60.Jv, 13.85.Ni, 14.80.Ly

## I. INTRODUCTION

Together with the possible existence of extra spatial dimensions, supersymmetry (SUSY) remains the prime candidate for physics beyond the standard model (SM). Among the many undisputed theoretical advantages of the minimal supersymmetric SM (MSSM), the intimate connection of this new space-time symmetry with electroweak symmetry breaking is of particular importance. The search for SM or MSSM Higgs bosons as well as for spin-0 and spin-1/2 partners of the SM fermions and gauge bosons are therefore often considered to be the most important tasks for present and future collider experiments.

For many years, the focus has been on minimal supergravity (mSUGRA) models, in which SUSY is broken by gravitational interactions and the lightest SUSY particle (LSP) is the photino or, more generally, the lightest of four neutralinos,  $\tilde{\chi}_1^0$ . Only around 1980 was it discovered that the SUSY partner of the spin-2 graviton, the massless spin-3/2 gravitino, does not necessarily couple to matter with gravitational strength only, but that its coupling can be enhanced to electroweak strength once SUSY is broken through the super-Higgs mechanism and the associated Goldstone fermion, the spin-1/2 goldstino, is absorbed to give the gravitino its mass and its longitudinal degrees of freedom, making it the LSP [1,2].

The electroweak strength of goldstino interactions with massless photons and photinos was then used to impose limits on the gravitino mass by comparing total theoretical cross sections for electron-positron colliders to experimental single-photon searches at SLAC PEP and DESY PETRA, resulting in a first mass limit of  $m_{\tilde{G}} \geq 2.3 \times 10^{-6}$  eV [3]. Subsequently, the single-photon searches at CERN LEP 1 and LEP 161 with cross section limits of 0.1 and 1 pb implied gravitino masses above  $10^{-3}$  and  $10^{-5}$  eV for light neutralinos of mass below 50 and 100 GeV, respectively [4]. These limits were, however, obtained without imposing missing or observed photon energy cuts on the theoretical cross section.

In 1988, the CDF Collaboration published a cross section limit of 100 pb for their monojet search at the Fermilab  $p\bar{p}$  collider Tevatron [5], which they used to impose bounds on the squark-gluino mass plane, but which could also be interpreted as the absence of a light (s)goldstino signal, yielding  $m_{\tilde{G}} > 2.2 \times 10^{-5}$  eV and  $m_{\tilde{g}} \geq 100$  GeV [6]. This first hadron-collider analysis assumed, however, very heavy squarks of  $m_{\tilde{q}} \geq 500$  GeV and was based on partonic subprocesses involving only gluons and gluinos, but no (s)quarks. The analysis was later reapplied to the 1996 CDF multijet cross section limit of 1.4 pb [7], yielding  $m_{\tilde{G}} \geq 3 \times 10^{-4}$  eV and  $m_{\tilde{g}} \geq 200$  GeV [8]. Predictions were also made for the CERN LHC, albeit for an assumed center-of-mass energy of 16 TeV [9].

While the gluon-gluon initial state dominates indeed for the production of light final states at the LHC, it is well

\*Electronic address: [klasen@lpsc.in2p3.fr](mailto:klasen@lpsc.in2p3.fr)

known that it is the quark-antiquark luminosity that dominates at the Tevatron and that quark-gluon-initiated QCD Compton processes contribute significantly for heavier final states at the LHC. A complete and robust study must therefore take into account (1) all partonic subprocesses leading to the production of single gravitinos, i.e.  $q\bar{q} \rightarrow \tilde{G}\tilde{g}$ ,  $gg \rightarrow \tilde{G}\tilde{g}$ , and  $qg \rightarrow \tilde{G}\tilde{q}$ , (2) the subsequent decay of the squark/gluino into an observed jet and a second gravitino, i.e.  $\tilde{g} \rightarrow \tilde{G}g$  and  $\tilde{q} \rightarrow \tilde{G}q$ , (3) up-to-date collider energies, parton density functions (PDFs), values of  $\Lambda_{\text{QCD}}$ , and SUSY-breaking scenarios, (4) the experimental cuts on the jet and missing transverse energies, and (5) the most recent experimental cross section limits.

In Sec. II, we calculate analytical gravitino production cross sections and decay widths using an effective supergravity Lagrangian in four-component notation (see Appendix A) and the Feynman rules for single gravitinos derived from it (see Appendix B). We discuss in some detail the gauge independence of our results and its relation to the sign of interferences and the presence of quartic vertices. In Sec. III, we first present a concise review of gauge-mediated SUSY-breaking (GMSB) models, where gravitinos are naturally the lightest SUSY particles, and discuss their implementation in different benchmark slopes. We then establish the regions in which gluino/squark decays into gravitinos and jets dominate. Next, we present the various subprocess contributions to the total cross sections at the Tevatron and LHC and compute the jet and missing transverse-momentum spectra, taking into account the gluino/squark decays. Finally, we deduce a new limit on the gravitino mass from the latest CDF monojet search and discuss the signal size and missing  $E_T$  trigger thresholds at the LHC. Our conclusions are presented in Sec. IV. The discussion of cosmological constraints on the gravitino mass is beyond the scope of this paper. For a recent analysis of Lyman- $\alpha$  forest and WMAP data, assuming a light gravitino as a warm dark matter candidate in GMSB models and yielding  $m_{\tilde{G}} \leq 16$  eV, we refer the reader to [10] and the references therein.

## II. ANALYTICAL RESULTS

In this section, we present our analytical results for the hadroproduction cross sections of single gravitinos with gluinos and squarks (Sec. II A) and the two-body decay widths of squarks and gluinos into gravitinos with quarks and gluons (Sec. II B). They have been obtained by using an effective supergravity Lagrangian in nonderivative form (see Appendix A), from which the corresponding Feynman rules (see Appendix B) have been derived.

### A. Production

In  $R$ -parity conserving supersymmetry, single gravitinos can be produced in strong interactions in association with

either gluinos or squarks. In addition, the associated production of gravitinos and gluinos proceeds through two competing initial states, i.e. quark-antiquark or gluon-gluon scattering, while gravitinos and squarks can only be produced in quark-gluon scattering due to fermion number conservation. The differential cross sections

$$\frac{d\hat{\sigma}}{dt} = \frac{1}{2s} \frac{1}{8\pi s} \overline{|M|^2} \quad (1)$$

depend, in general, on the SUSY particle masses; the usual Mandelstam variables  $s$ ,  $t$ , and  $u$ ; and their mass-subtracted counterparts,  $t_{\tilde{q},\tilde{g}} = t - m_{\tilde{q},\tilde{g}}^2$  and  $u_{\tilde{q},\tilde{g}} = u - m_{\tilde{q},\tilde{g}}^2$ . The gravitino mass  $m_{\tilde{G}}$  will be neglected everywhere except in the coupling constants, so that  $t$  is integrated over the interval  $[-s + m_{\tilde{q},\tilde{g}}^2; 0]$ .

We first consider the process initiated by quarks and antiquarks,

$$q\bar{q} \rightarrow \tilde{G}\tilde{g}, \quad (2)$$

whose contributing Feynman diagrams are shown in Fig. 1. The corresponding squared transition matrix element, averaged (summed) over initial (final) state spins and colors and summed over left- and right-handed squark exchanges,

$$\begin{aligned} \overline{|M|^2}_{q\bar{q} \rightarrow \tilde{G}\tilde{g}} = & \frac{g_s^2 C_F}{3N_C M^2 m_{\tilde{G}}^2} \left[ \frac{m_{\tilde{g}}^2}{s} (2tu - m_{\tilde{g}}^2(t+u)) + \frac{m_{\tilde{q}}^4}{t_{\tilde{q}}^2} tt_{\tilde{g}} \right. \\ & \left. + \frac{m_{\tilde{q}}^4}{u_{\tilde{q}}^2} uu_{\tilde{g}} + \frac{2m_{\tilde{g}}^2 m_{\tilde{q}}^2}{t_{\tilde{q}} u_{\tilde{q}}} (-2tu + m_{\tilde{q}}^2(t+u)) \right], \quad (3) \end{aligned}$$

is symmetric under the exchange of the  $t$  and  $u$  Mandelstam variables. The  $s$ -channel contribution is individually gauge independent, and the  $t$ - and  $u$ -channel contributions are manifestly gauge independent. For gluino

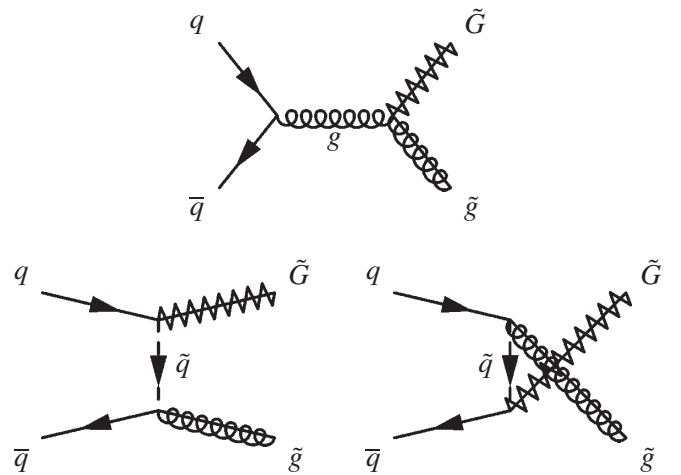


FIG. 1. Leading-order Feynman diagrams for the production of a gravitino in association with a gluino in quark-antiquark collisions.

pair production, an interference term between the  $t$ - and  $u$ -channel diagrams proportional to the squared gluino mass exists [11], but this term vanishes for gravitino-gluino associated production linearly with the gravitino mass.

The contributions from individual diagrams that we obtain differ, of course, from those presented in Eq. (4) of [12], since our effective Feynman rules are proportional to the SUSY particle masses, but our total results agree. A related cross section has been computed with effective Feynman rules in Eq. (28) of [4] for the associated production of gravitinos and neutralinos at lepton colliders. After adjustment of masses, couplings, and color factors, it agrees with our result. In the limit of negligible squark and gluino masses, where the  $t$ - and  $u$ -channel contributions both vanish due to the higher mass dimension of the squark coupling, our result agrees also with Table 1 in [13] when summed over left- and right-handed quarks. This limit is, however, only applicable in the high-energy context of cosmology [13] and not at current hadron colliders.

Next, we compute the competing gluon-initiated process

$$gg \rightarrow \tilde{G} \tilde{g}, \quad (4)$$

whose contributing Feynman diagrams are shown in Fig. 2. The gauge-independent total squared matrix element

$$\begin{aligned} \overline{|M|}_{gg \rightarrow \tilde{G} \tilde{g}}^2 &= \frac{g_s^2 m_{\tilde{g}}^2}{6C_F M^2 m_{\tilde{G}}^2} \frac{stu}{s^2 t_{\tilde{g}}^2 u_{\tilde{g}}^2} [tu(t^2 + u^2) \\ &\quad - m_{\tilde{g}}^2(t^3 + 6t^2u + 6tu^2 + u^3) \\ &\quad + 2m_{\tilde{g}}^4(2t^2 + 7tu + 2u^2) - 5m_{\tilde{g}}^6(t + u)], \end{aligned} \quad (5)$$

averaged (summed) over initial (final) state spins and colors, is again symmetric under interchange of the final gravitino and gluino and consequently also of the Mandelstam variables  $t$  and  $u$ . Our result agrees with Eq. (6) in [12] and also with Table 1 in [13] in the limit of small gluino mass. It also agrees with Eq. (5) in [8], if its

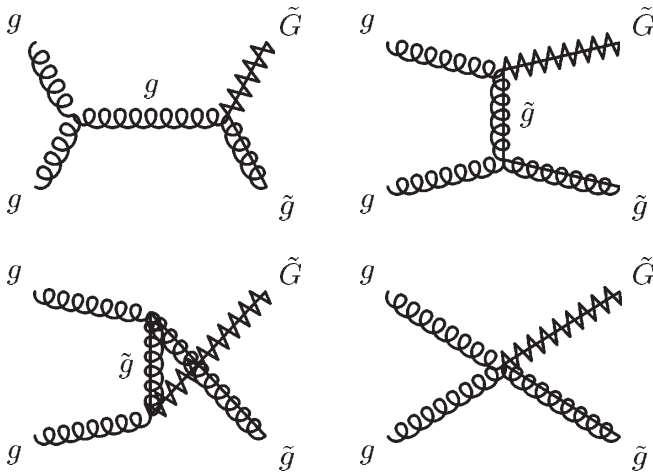


FIG. 2. Leading-order Feynman diagrams for the production of a gravitino in association with a gluino in gluon-gluon collisions.

variables  $t$  and  $u$  are understood to be their mass-subtracted counterparts and if its integration variable  $z$ , whose definition is unfortunately missing, is assumed to be given by  $z = 1 + 2t/(s - m_{\tilde{g}}^2) \in [-1; 1]$ .

Finally, we analyze the associated production of gravitinos and squarks, which is initiated by quark-gluon scattering,

$$qg \rightarrow \tilde{G} \tilde{q}_i, \quad (6)$$

and proceeds through the Feynman diagrams in Fig. 3. In this case, the squared matrix element for a squark of a given chirality  $i$  is

$$\begin{aligned} \overline{|M|}_{qg \rightarrow \tilde{G} \tilde{q}_i}^2 &= \frac{g_s^2}{12N_C M^2 m_{\tilde{G}}^2} \left[ \frac{m_{\tilde{q}_i}^4}{st_{\tilde{q}_i}^2} (-u)(t^2 + m_{\tilde{q}_i}^4) \right. \\ &\quad \left. + \frac{m_{\tilde{g}}^2}{u_{\tilde{g}}^2} (-u)(tu + m_{\tilde{g}}^2 s) + \frac{m_{\tilde{g}}^2 m_{\tilde{q}_i}^4}{t_{\tilde{q}_i} u_{\tilde{g}}^2} (2u) \right], \end{aligned} \quad (7)$$

where the first term in the square brackets denotes the gauge-independent sum of  $s$ - and  $t$ -channel contributions including their interference, while the  $u$ -channel contribution in the second term is individually gauge independent. The third term corresponds to the gauge-independent sum of  $s$ - and  $t$ -channel interferences with the  $u$ -channel. The same result is obtained for the charge-conjugated process,

$$\bar{q}g \rightarrow \tilde{G} \tilde{q}_i^*. \quad (8)$$

This leads to a factor of 2 for  $p\bar{p}$  colliders with a neutral initial state such as the Tevatron, but not for  $pp$  colliders such as the LHC, where the parton densities are not charge symmetric. Our result agrees with the one in [12], which has been obtained with derivative couplings including a quark-gluon-gravitino-squark vertex contribution. Note that this quartic vertex is absent in the effective theory [14], since it would spoil the gauge independence. At high

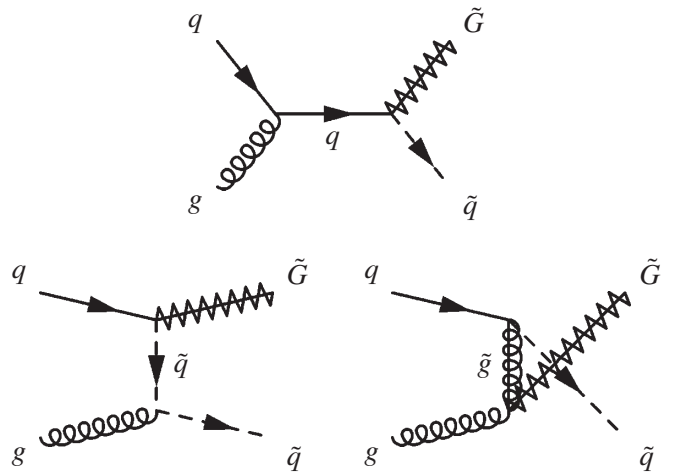


FIG. 3. Leading-order Feynman diagrams for the production of a gravitino in association with a squark in quark-gluon collisions.

energies, only the  $u$ -channel contribution survives, so that our result agrees with the one in Table 1 of [13].

### B. Decay

Heavy squarks and gluinos may decay either directly or through cascades into the lightest SUSY particle, which we assume to be the gravitino. Direct decays, which dominate for light gravitinos [6], proceed through the Feynman diagrams shown in Fig. 4, and the corresponding partial widths

$$\frac{d\Gamma}{dt} = \frac{1}{2m_{\tilde{q},\tilde{g}}} \frac{1}{8\pi m_{\tilde{q},\tilde{g}}^2} |\overline{M}|^2 \quad (9)$$

are obtained from the squared transition matrix elements after integration of the Mandelstam variable  $t$  over the interval  $[-m_{\tilde{q},\tilde{g}}^2 + m_q^2; 0]$ . For a squark of a given chirality  $i$ , the squared matrix element

$$|\overline{M}|_{\tilde{q}_i \rightarrow \tilde{G}q}^2 = \frac{(m_{\tilde{q}_i}^2 - m_q^2)^3}{3M^2 m_{\tilde{G}}^2} \quad (10)$$

leads then to the partial width

$$\Gamma_{\tilde{q}_i \rightarrow \tilde{G}q} = \frac{m_{\tilde{q}_i}^5}{48\pi M^2 m_{\tilde{G}}^2} \left(1 - \frac{m_q^2}{m_{\tilde{q}_i}^2}\right)^4. \quad (11)$$

Since the gluon mass is, of course, zero ( $m_g = 0$ ), the squared gluino decay matrix element, averaged (summed) over initial (final) spins, is

$$|\overline{M}|_{\tilde{g} \rightarrow \tilde{G}g}^2 = \frac{m_{\tilde{g}}^6}{3M^2 m_{\tilde{G}}^2}, \quad (12)$$

leading to the partial width

$$\Gamma_{\tilde{g} \rightarrow \tilde{G}g} = \frac{m_{\tilde{g}}^5}{48\pi M^2 m_{\tilde{G}}^2}. \quad (13)$$

These results are well known [15]. They agree, in particular, with the general result in Eq. (6.24) of [16], valid for the decay of any heavier SUSY particle into its standard model partner and a lighter gravitino.

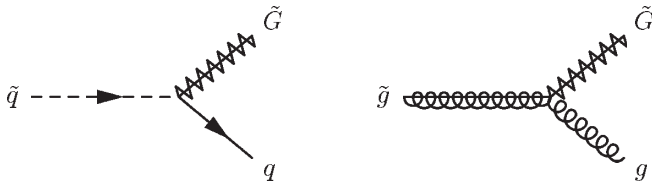


FIG. 4. Leading-order Feynman diagrams for the decay of a squark into a gravitino and a quark (left diagram) and a gluino into a gravitino and a gluon (right diagram).

## III. NUMERICAL RESULTS

### A. Gauge-mediated supersymmetry breaking

In GMSB models, SUSY breaking occurs in a secluded sector at the scale  $\langle F \rangle$ , related to the gravitino mass by  $m_{\tilde{G}} = \langle F \rangle / (\sqrt{3}M)$ , and is transmitted to the observable sector by a chiral superfield  $S$  and  $n_q$  quarklike and  $n_l$  leptonlike messenger fields [16,17]. The superfield  $S$  is a gauge singlet, but its scalar and auxiliary components overlap with the gravitino and acquire vacuum expectation values  $\langle S \rangle$  and  $\langle F_S \rangle$ . The messenger fields then acquire a mass  $M_{\text{mess}} \simeq \langle S \rangle$  through Yukawa couplings to the superfield  $S$ . They are given the same standard model gauge couplings to the observable fields as ordinary quarks and leptons, so that they can induce gaugino and sfermion masses through one- and two-loop self-energy diagrams, respectively. The lightest SUSY particle is always the gravitino, and it is for this reason that we concentrate our numerical study of gravitino production at hadron colliders on GMSB scenarios.

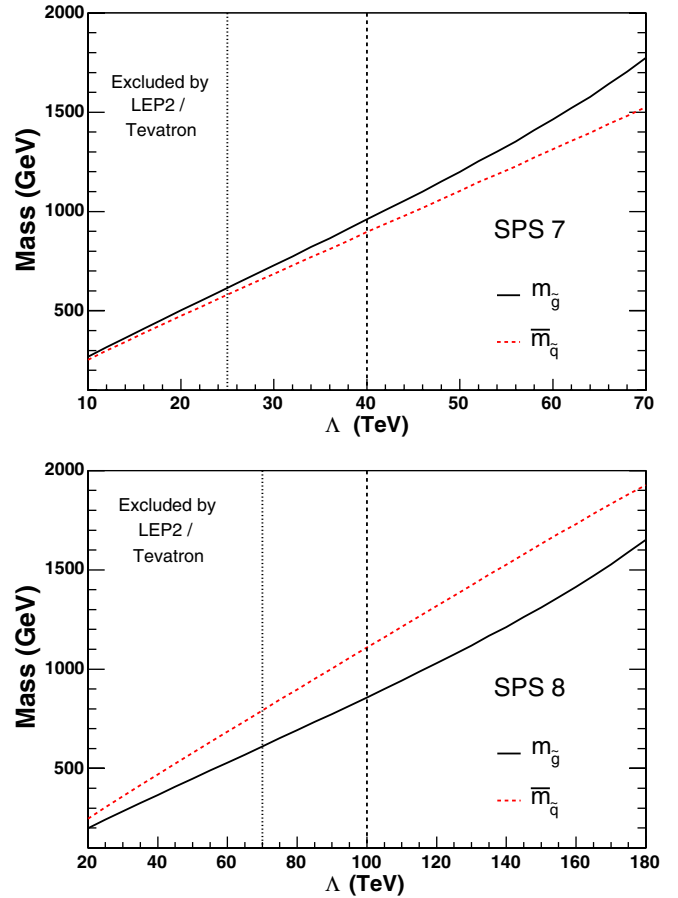


FIG. 5 (color online). Average squark and physical gluino masses for the GMSB benchmark slopes SPS 7 (top panel) and SPS 8 (bottom panel) as a function of the effective SUSY-breaking scale  $\Lambda$ , with  $M_{\text{mess}}/\Lambda = 2$ ,  $\tan\beta = 15$ , and  $\mu > 0$  fixed.



Besides  $M_{\text{mess}}$ ,  $n_q$ , and  $n_l$ , GMSB scenarios are determined by the ratio of Higgs vacuum expectation values  $\tan\beta$ , the sign of the Higgs mass parameter  $\mu$ , and by the auxiliary vacuum expectation value  $\langle F_S \rangle$ , which is related to the mass splitting of the messenger fields and realistically considerably smaller than both the squared mass scale of the messenger fields,  $\langle S \rangle^2$ , and the fundamental SUSY-breaking scale  $\langle F \rangle$ . It is usually reexpressed in terms of an effective SUSY-breaking scale,  $\Lambda = \langle F_S \rangle / \langle S \rangle$ .

A number of SUSY benchmark scenarios have been proposed in [18] in order to facilitate detailed comparisons between SUSY searches at different colliders and with different signals/backgrounds. In particular, we show in Fig. 5 the average squark and physical gluino masses for the two GMSB scenarios proposed in [18], SPS 7 and 8, as a function of the effective SUSY-breaking scale  $\Lambda$ , with  $M_{\text{mess}}/\Lambda = 2$ ,  $\tan\beta = 15$ , and  $\mu > 0$  fixed. For SPS 7, the benchmark point (indicated by a vertical dashed line) is at  $\Lambda = 40$  TeV and  $n_q = n_l = 3$ , leading to a stau ( $\tilde{\tau}_1$ ) next-to-lightest SUSY particle (NLSP), while for SPS 8, the benchmark point is at  $\Lambda = 100$  TeV and  $n_q = n_l = 1$ , leading to a neutralino ( $\tilde{\chi}_1^0$ ) NLSP. The regions that have already been excluded by LEP2 and Tevatron searches for light neutralinos and charginos in GMSB scenarios lie to the left of the vertical dotted line [19]. The physical masses in Fig. 5 have been obtained by imposing boundary conditions at the grand unification theory (GUT) scale and evolving them to the electroweak symmetry breaking scale via renormalization group equations using the computer program SUSPECT [20]. Note that the mass hierarchy of gluinos and squarks at SPS 7,  $m_{\tilde{g}} \geq \tilde{m}_{\tilde{q}}$ , is reversed at SPS 8, where  $m_{\tilde{g}} \leq \tilde{m}_{\tilde{q}}$ .

## B. Branching ratios

We are now in a position to determine the regions in SUSY parameter space where the squarks and gluinos, that are produced in association with the gravitino at hadron colliders, decay dominantly into a two-body final state with a second gravitino and a quark or gluon, leading to an experimentally identifiable monojet signal with large missing transverse energy.

To this end, we evaluate the decay widths  $\Gamma_{\tilde{G}}$  calculated in Sec. II B in the GMSB scenarios discussed in Sec. III A and compare them to the competing total decay width  $\Gamma_{\text{MSSM}}$  of gluinos and squarks into MSSM two-body final states up to one-loop level and those into three- and four-body final states at tree level as implemented in the computer program SDECAY [21]. The resulting branching ratios,

$$\text{BR} = \frac{\Gamma_{\tilde{G}}}{\Gamma_{\text{MSSM}} + \Gamma_{\tilde{G}}}, \quad (14)$$

of gluinos and squarks are shown in Figs. 6 and 7 as a function of the gravitino mass and of the effective SUSY-breaking scale  $\Lambda$ , defining the GMSB benchmark slopes SPS 7 (top panel) and SPS 8 (bottom panel).

For both benchmark points, we observe that left- and right-handed, up- and down-type squarks decay dominantly with  $\text{BR} \geq 0.9$  into gravitinos, if the gravitino mass does not exceed  $m_{\tilde{G}} \leq 10^{-4}$  eV. While the SUSY-breaking scale  $\Lambda$  must not lie significantly below the benchmark points of  $\Lambda = 40$  and 100 TeV, respectively, these regions are already largely excluded by LEP2 and Tevatron searches for light neutralinos and charginos in GMSB scenarios [19].

For gluinos, the conclusions are quite similar for SPS 7, but more optimistic for SPS 8 with the decay into gravitinos dominating up to  $m_{\tilde{G}} \leq 10^{-3}$  eV for all physical values of  $\Lambda$ . Above these limits, the decay chains depend essentially on the mass hierarchy of the SUSY spectrum with  $\tilde{g} \rightarrow \tilde{q}q$  and  $\tilde{q} \rightarrow \tilde{\chi}_i^{0,\pm} q^{(\prime)}$  at SPS 7, whereas  $\tilde{q} \rightarrow \tilde{g}q$  and  $\tilde{g} \rightarrow \tilde{\chi}_i^{0,\pm} q\bar{q}^{(\prime)}$  at SPS 8, leading, in general, to more complicated multijet signals. Note that all of these decays are instantaneous with decay lengths around or below 1 fm, so that they occur close to the primary vertex and well inside any collider detector.

While our numerical results for squark decays are new, gluino decays were studied quite some time ago in a simple

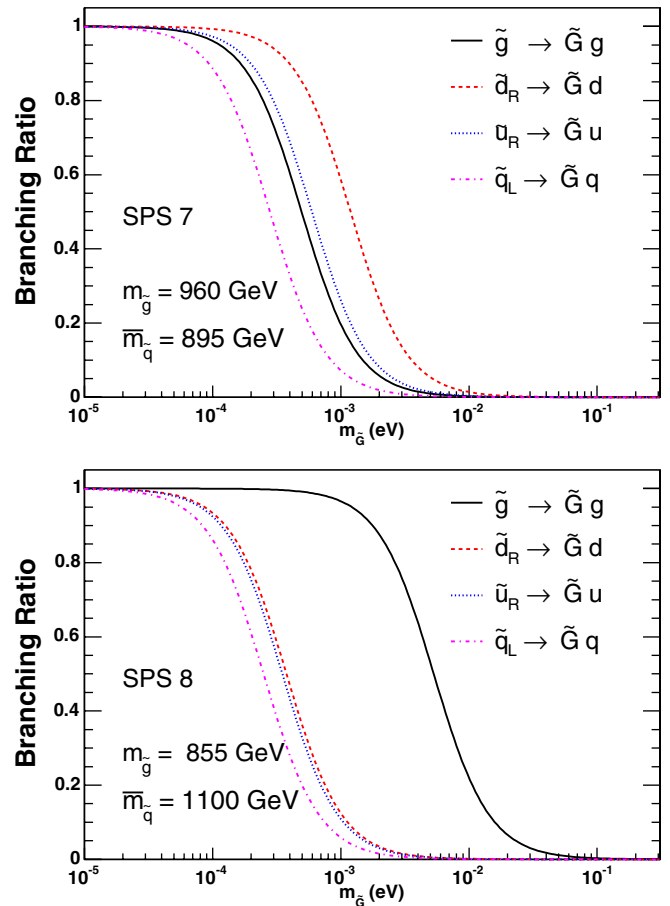


FIG. 6 (color online). Branching ratios of gluinos/squarks into gravitinos and gluons/quarks as a function of the gravitino mass with the other SUSY masses fixed to their SPS 7 (top panel) and SPS 8 (bottom panel) GMSB benchmark values.

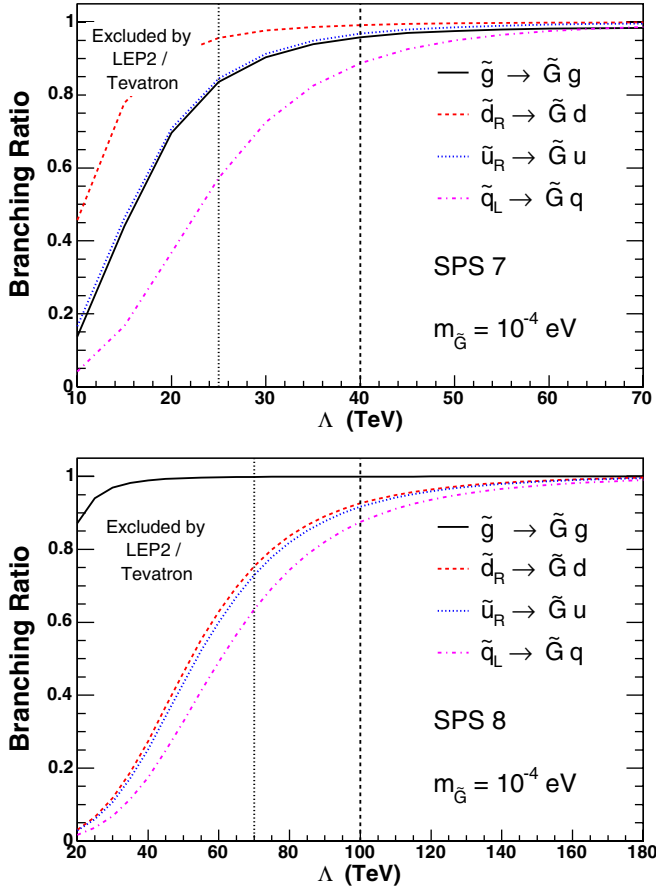


FIG. 7 (color online). Branching ratios of gluinos/squarks into gravitinos and gluons/quarks for  $m_{\tilde{G}} = 10^{-4}$  eV and the GMSB benchmark slopes SPS 7 (top panel) and SPS 8 (bottom panel) as a function of the effective SUSY-breaking scale  $\Lambda$ .

SUSY scenario with a massless photino NLSP. In Fig. 1 of [6], the two-body decay  $\tilde{g} \rightarrow \tilde{G}g$  has been compared with the tree-level three-body decay  $\tilde{g} \rightarrow \tilde{\gamma}q\bar{q}$ , neglecting all other decay modes and for  $m_{\tilde{g}} = 100$  GeV and  $m_{\tilde{q}} = 500$  GeV. The conclusion there was that  $\text{BR} \geq 0.9$  up to  $m_{\tilde{G}} \leq 10^{-4}$  eV, which compares quite favorably with our result at SPS 8 and  $\Lambda = 20$  TeV (see the lower part of Fig. 7), where the masses  $m_{\tilde{g}} = 200$  GeV,  $m_{\tilde{q}} = 250$  GeV, and  $m_{\tilde{\chi}_1^0} = 14$  GeV are of similar magnitude. For  $m_{\tilde{q}} = 1000$  GeV, the gravitino decay mode was found to dominate up to  $m_{\tilde{G}} = 5 \times 10^{-3}$  eV (see Fig. 1 of [8]). This compares again favorably with our result at the benchmark point SPS 8 (see the lower panel of Fig. 6), where  $m_{\tilde{q}} = 1100$  GeV. Related results for a massless photino NLSP and gluino masses between 200 and 750 GeV and squark masses between 500 and 2000 GeV can furthermore be found in Fig. 1 of [9].

### C. Tevatron

The total hadronic cross section for gravitino-gluino or gravitino-squark associated production,

$$\sigma = \int_{m^2/S}^1 d\tau \int_{-1/2\ln\tau}^{1/2\ln\tau} dy \int_{t_{\min}}^{t_{\max}} dt \sum_{a,b} f_{a/A}(x_a, M_a^2) \times f_{b/B}(x_b, M_b^2) \frac{d\hat{\sigma}_{ab}}{dt}, \quad (15)$$

can be obtained by convolving the partonic cross sections  $d\hat{\sigma}_{ab}/dt$  presented in Sec. II A with the parton density functions (PDFs)  $f_{a,b/A,B}$  at the factorization scale  $M_{a,b}$ . Since the PDFs vanish rapidly, as the longitudinal momentum fractions  $x_{a,b}$  of the partons  $a, b$  in the external hadrons  $A, B$  approach unity, the available partonic center-of-mass energy  $s = x_a x_b S$  represents only a fraction  $\tau = x_a x_b$  of hadronic center-of-mass energy  $S$ , and the experimentally accessible mass range for searches of new SUSY particles is naturally limited. We consider the initial gluons and five light quarks to be massless and denote the average final state mass by  $m$ . At the LHC, both  $A$  and  $B$  represent protons, which will collide with  $\sqrt{S} = 14$  TeV starting in 2008, whereas at the Tevatron,  $B$  represents an antiproton beam with  $\sqrt{S} = 1.8$  TeV at the completed run I and 1.96 TeV at the current run II.

Numerical predictions for single-gravitino hadroproduction cross sections at run I of the Tevatron have been presented in Figs. 4, 5, and 6 of [12] as a function of  $m_{\tilde{g}}$  and  $m_{\tilde{q}}$ , respectively. We have verified these results by fixing the strong coupling to its world-average value  $\alpha_s(M_Z) = 0.118$  and convolving our partonic cross sections in Sec. II A with the (nowadays obsolete) set of PDFs of [22], evolved from the starting scale  $Q_0 = 2$  GeV and using a value of  $\Lambda_{\text{LO}}^{n_f=5} = 144$  MeV to the factorization scale  $M_a = M_b = m_{\tilde{g},\tilde{q}}$ . In the following, we will, however, use the modern PDFs of CTEQ6L1 [23], which correspond to a one-loop running of the strong coupling  $\alpha_s(\mu) = g_s^2/(4\pi)$  and a QCD scale parameter of  $\Lambda_{\text{LO}}^{n_f=5} = 165$  MeV, derived from the world-average value of  $\alpha_s(M_Z) = 0.118$  [19]. The renormalization scale  $\mu$  and the factorization scales  $M_{a,b}$  will be fixed to the average particle mass  $m = (m_{\tilde{G}} + m_{\tilde{q},\tilde{g}})/2$  in the final state.

In Fig. 8, the total cross section of the associated production of gravitinos and gluinos or squarks is shown for the GMSB benchmark scenarios SPS 7 (top panel) and 8 (bottom panel) and a gravitino mass of  $m_{\tilde{G}} = 10^{-5}$  eV as a function of the effective SUSY-breaking scale  $\Lambda$ . While the quark-gluon-initiated production of gravitinos and squarks can contribute significantly to the total event sample for SPS 7, where  $m_{\tilde{q}} \leq m_{\tilde{g}}$ , the largest contribution at SPS 7, and even more so at SPS 8, where  $m_{\tilde{g}} \leq m_{\tilde{q}}$ , comes from the subprocess  $q\bar{q} \rightarrow \tilde{G}\tilde{g}$ . This is, of course, due to the large quark-antiquark luminosity at the Tevatron. At run II, where the integrated luminosity has already reached  $2.6 \text{ fb}^{-1}$  and is expected to increase to  $4.4$  to  $8.8 \text{ fb}^{-1}$  until the final shutdown in 2009 [24], the CDF and D0 experiments should be able to discover light gravitinos with masses up to  $10^{-5}$  eV in events with a single jet and large

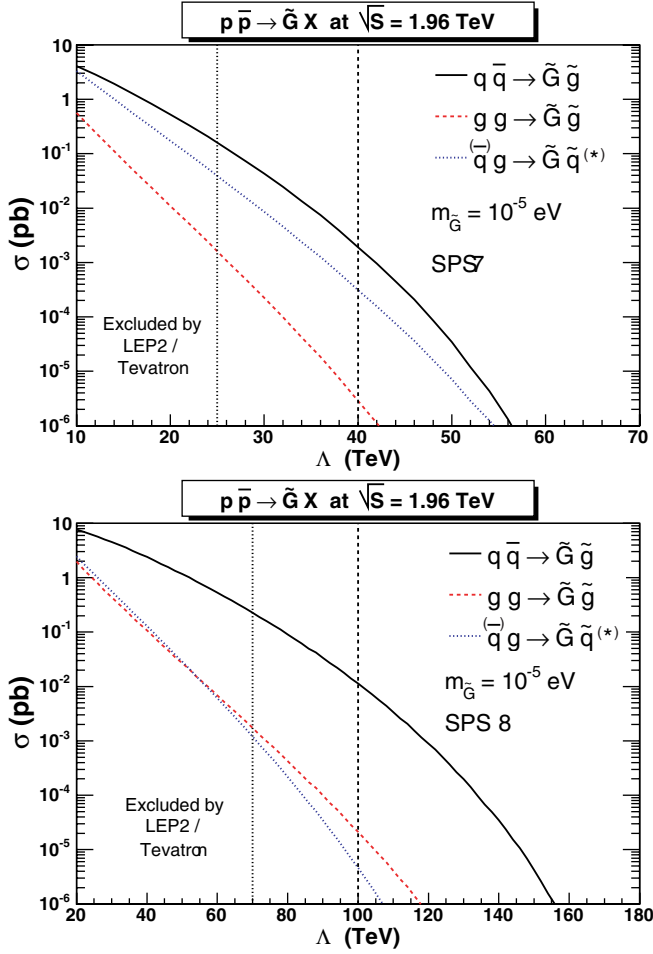


FIG. 8 (color online). Total cross sections of gravitino and gluino/squark associated production at run II of the Tevatron for  $m_{\tilde{G}} = 10^{-5}$  eV and the GMSB benchmark slopes SPS 7 (top panel) and SPS 8 (bottom panel) as a function of the effective SUSY-breaking scale  $\Lambda$ .

missing transverse energy for values of  $\Lambda$  above the current exclusion limits (25 and 70 TeV for SPS 7 and 8, respectively). If we assume the large- $E_T$  monojet signal to have very little SM background (see Fig. 9 below) and thus to be experimentally identifiable with high efficiency, we can define the visible region by the point where the total cross section falls to 1 fb, so that only a few events will be recorded. The discovery reach then extends up to the benchmark point (40 TeV) at SPS 7, where  $m_{\tilde{g}} = 950$  GeV and  $\tilde{m}_{\tilde{q}} = 890$  GeV, and even up to 120 TeV at SPS 8, where  $m_{\tilde{g}} = 1000$  GeV and  $\tilde{m}_{\tilde{q}} = 1300$  GeV. For lighter gravitino masses, the total cross section scales trivially according to Eqs. (3), (5), and (7), i.e. with the inverse of the squared gravitino mass.

For a detailed, model-independent account of the experimentally identifiable monojet signal of the associated production of a gravitino with a squark or gluino, we have to include the decay of the latter into a second gravitino and an observed jet. If we continue to neglect  $m_{\tilde{G}}$ , except in the

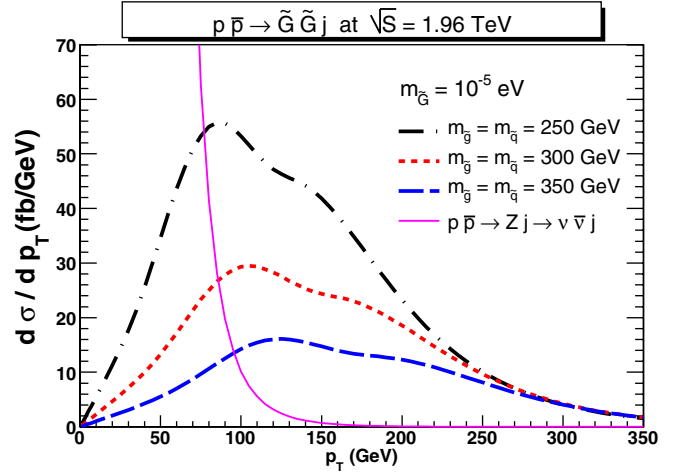


FIG. 9 (color online). Transverse-momentum spectra of the observed jet in gravitino production at run II of the Tevatron for  $m_{\tilde{G}} = 10^{-5}$  eV and three different squark/gluino masses. Also shown is the main SM background from invisible Z-boson decays.

coupling, the cross section for a massless three-body final state can be written as

$$\begin{aligned}
 d\sigma &= \frac{1}{2s} \int f_{a/A}(x_a, M_a^2) dx_a f_{b/B}(x_b, M_b^2) \\
 &\times dx_b |\overline{M}|_{2 \rightarrow 3}^2 (2\pi)^4 \delta^4\left(p_a + p_b - \sum_{i=1}^3 p_i\right) \\
 &\times \prod_{i=1}^3 \frac{d^3 p_i}{(2\pi)^3 2E_i} = \frac{1}{2s} \int f_{a/A}(x_a, M_a^2) \\
 &\times f_{b/B}(x_b, M_b^2) |\overline{M}|_{2 \rightarrow 3}^2 (2\pi)^{-5} \\
 &\times \frac{p_{T_1}}{2} d p_{T_1} d \eta_1 d \phi_1 \frac{p_{T_2}}{2} d p_{T_2} d \eta_2 d \phi_2 \frac{1}{S} d \eta_3, \quad (16)
 \end{aligned}$$

where  $p_{T_1}$  represents the observed jet transverse momentum, which is balanced by the missing transverse momentum of the two gravitinos. Since the squark or gluino decay width is of the order of  $\hbar c/1 \text{ fm} = 0.2 \text{ GeV}$  (see Sec. III B), we can apply the narrow-width approximation to rewrite the squared and averaged  $2 \rightarrow 3$  scattering matrix element as

$$\begin{aligned}
 |\overline{M}|_{2 \rightarrow 3}^2 &= |\overline{M}|_{2 \rightarrow 2}^2 \left| \frac{1}{s_{12} - m_{\tilde{q}, \tilde{g}}^2 + i m_{\tilde{q}, \tilde{g}} \Gamma_{\tilde{q}, \tilde{g}}} \right|^2 |\overline{M}|_{1 \rightarrow 2}^2 \\
 &\rightarrow |\overline{M}|_{2 \rightarrow 2}^2 \frac{\pi \delta(s_{12} - m_{\tilde{q}, \tilde{g}}^2)}{m_{\tilde{q}, \tilde{g}} \Gamma_{\tilde{q}, \tilde{g}}} |\overline{M}|_{1 \rightarrow 2}^2. \quad (17)
 \end{aligned}$$

By fixing the azimuthal angle of the observed jet to  $\phi_1 = 0$ , the squared invariant mass of the intermediate squark/gluino propagator becomes

$$s_{12} = 2p_{T_1} p_{T_2} (\cosh \eta_1 \cosh \eta_2 - \sinh \eta_1 \sinh \eta_2 - \cos \phi_2), \quad (18)$$

so that

$$\delta(s_{12} - m_{\tilde{q},\tilde{g}}^2) = \frac{\delta[\phi_2 - \arccos(\cosh\eta_1 \cosh\eta_2 - \sinh\eta_1 \sinh\eta_2 - \frac{m_{\tilde{q},\tilde{g}}^2}{2p_{T_1} p_{T_2}})]}{p_{T_1} p_{T_2} |\sin\phi_2|}. \quad (19)$$

The three-body cross section

$$d\sigma = \int x_a f_{a/A}(x_a, M_a^2) x_b f_{b/B}(x_b, M_b^2) \frac{d\hat{\sigma}}{dt} \times \text{BR}(\tilde{q}, \tilde{g} \rightarrow \tilde{G}X) \frac{2}{\pi |\sin\phi_2|} dp_{T_1} d\eta_1 dp_{T_2} d\eta_2 d\eta_3 \quad (20)$$

can then be expressed in terms of the squared and averaged  $2 \rightarrow 2$  production cross section of gravitinos and squarks or gluinos,  $d\hat{\sigma}/dt$  (see Sec. II A), and the squark or gluino branching ratio  $\text{BR}(\tilde{q}, \tilde{g} \rightarrow \tilde{G}X)$  into a gravitino and a jet (see Sec. II B).

The transverse-momentum spectrum of the observed jet, which is equivalent to the missing transverse-momentum spectrum, is shown in Fig. 9 for the same gravitino mass of  $10^{-5}$  eV as in Fig. 8. At this point, squarks and gluinos always decay into gravitinos and jets (see Fig. 6). Their decay widths vary between 4% and 17% of their masses, as these increase from the current exclusion limit of 250 GeV to 350 GeV, so that the narrow-width approximation is always justified. All three spectra peak at values slightly below half of the squark/gluino mass, as expected from kinematic considerations. The main SM background, which comes from the associated production of a jet and a Z-boson, followed by an invisible Z decay, peaks at roughly half the Z-boson mass. It can be eliminated by cutting on the invisible (or jet) transverse momentum at values around 100 GeV.

In a recent analysis of run-I Tevatron data, the CDF Collaboration has examined events with a single jet and a missing transverse energy of at least 100 GeV [25]. From Fig. 9 it is clear that, while this cut eliminates basically all of the soft-QCD and other standard model backgrounds, only little signal cross section is lost. For an optimized missing transverse-energy cut of 175 GeV, the CDF Collaboration found an upper limit of the gravitino cross section of 3.1 pb, corresponding to a gravitino mass of at most  $1.1 \times 10^{-5}$  eV. Note, however, that this analysis was done under the assumption that all other supersymmetric particles are heavy [26].

We therefore repeat the CDF analysis for general SUSY scenarios, using the 95% confidence limits on the product of the acceptance ( $A$ ) times the signal cross section ( $\sigma$ ) as a function of missing  $E_T$  as published in Fig. 3 of Ref. [25]. These limits are divided by the detector acceptance ( $A = 0.4$ ) for the selected data sample, assumed to have little dependence on the missing  $E_T$  [27]. The dependence of the number of simulated signal events on the varying missing- $E_T$  cut is then taken into account explicitly by

integrating Eq. (20) over  $p_{T_1} \geq 100, \dots, 300$  GeV. We also implement the experimental requirement that at least one jet lies in the central region,  $|\eta| \leq 0.7$ , since this cut is stricter than the additional CDF cut on the hardest jet to lie in  $|\eta| \leq 2.4$ , and our parton-level analysis has only one jet. We have verified that the number of events with a hard jet in the region  $0.7 \leq |\eta| \leq 2.4$  is indeed negligible.

From our confirmation of Figs. 5 and 6 in [12] we know that the two production processes that involve both the squark and gluino mass ( $q\bar{q} \rightarrow \tilde{G}\tilde{g}$  and  $qg \rightarrow \tilde{G}\tilde{q}$ ) are bounded from below for  $m_{\tilde{q}} = m_{\tilde{g}}$ , while the third production process  $gg \rightarrow \tilde{G}\tilde{g}$  depends only on the gluino mass. We therefore sum over all three production subprocesses with  $m_{\tilde{q}} = m_{\tilde{g}}$  and take  $\text{BR} = 1$  for  $m_{\tilde{G}} \leq 10^{-4}$  eV according to Fig. 6.

By always imposing the strongest experimental limit on  $A\sigma(\cancel{E}_T)$  of Fig. 3 in Ref. [25], divided by  $A = 0.4$  [27], on the correspondingly integrated cross section, Eq. (20), we obtain a contour in the  $m_{\tilde{G}}-m_{\tilde{g},\tilde{q}}$  plane, which is shown in Fig. 10 (solid curve). For light squark and gluino masses of 200 GeV, we find a gravitino mass limit of  $2 \times 10^{-5}$  eV that is very similar to that found by CDF for very heavy squarks and gluinos (dashed line). The limit in Fig. 10 degrades slowly to  $4 \times 10^{-6}$  eV as the squark/gluino mass increases to 700 GeV, i.e. as it approaches the center-of-

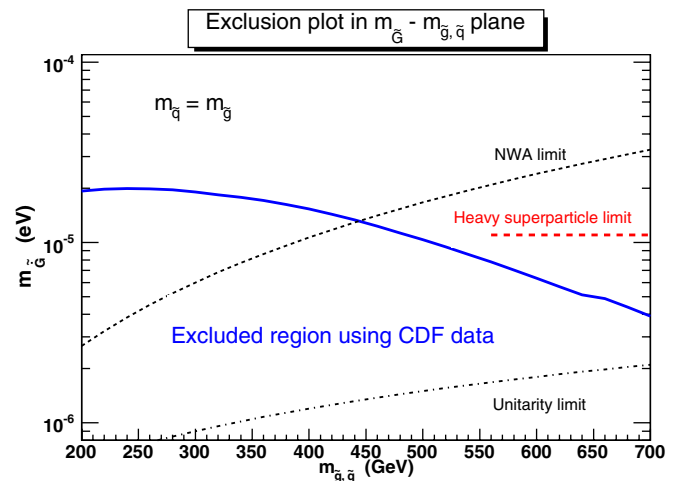


FIG. 10 (color online). Exclusion contour (solid curve) in the  $m_{\tilde{G}}-m_{\tilde{g},\tilde{q}}$  plane derived from the CDF acceptance times cross section limits for events with a single jet and varying missing transverse energy [25,27]. Also shown are the validity region of the narrow-width approximation (NWA, above the dotted curve), the CDF limit obtained for very heavy squarks and gluinos (dashed line), and the unitarity limit (dot-dashed line).



mass energy available at the Tevatron and the theoretical cross section falls. At the same time, the squark/gluino width increases and eventually passes the value of 1/4 of the squark/gluino mass (dotted curve in Fig. 10). Our results, obtained in the narrow-width approximation for single-gravitino production in association with relatively light squarks and gluinos, are thus complementary to those obtained by CDF for very heavy squarks and gluinos and double-gravitino production [25]. We have also checked that for our analysis, which is based on a single-gravitino effective Lagrangian, tree-level unitarity is always satisfied [28], since

$$\frac{m_{\tilde{G}}}{10^{-6} \text{ eV}} \geq 0.3 \frac{m_{\tilde{g}}}{100 \text{ GeV}} \quad (21)$$

for a critical energy corresponding to the Tevatron center-of-mass energy (dot-dashed curve in Fig. 10).

Two other experimental analyses of monojet signals at the Tevatron have been published, one based on 78.8 pb<sup>-1</sup> of run-I data by the D0 Collaboration [29] and one based on 368 pb<sup>-1</sup> of run-II data by the CDF Collaboration [30]. However, both analyses are interpreted with extra-dimensional models and directly present limits on the number of these extra dimensions and on the corresponding fundamental Planck scale. It would be interesting to reinterpret these analyses in the context of gravitino production. The CDF analysis quotes indeed a model-independent limit on signal events (or signal cross section times acceptance), but neither publication gives numerical values for detector acceptances. These were also not available from the collaborations upon request, so that we cannot at this point deduce independent gravitino mass limits from these data.

#### D. LHC

The high center-of-mass energy of  $\sqrt{S} = 14$  TeV and the large luminosity of initially 10 fb<sup>-1</sup> and finally 300 fb<sup>-1</sup> available at the LHC will provide the opportunity to test the soft SUSY-breaking hypothesis up to the multi-TeV range. This general remark remains true for the gauge-mediated SUSY-breaking scenarios SPS 7 (top panel) and 8 (bottom panel) with a gravitino LSP that we consider in Fig. 11. In this figure, we show the total cross sections of gravitino and gluino/squark associated production at the LHC for  $m_{\tilde{G}} = 10^{-4}$  eV and the three different partonic gravitino production processes discussed above. Their hierarchy is now opposite to the one at the Tevatron, i.e. it is the gluon luminosity that dominates and no longer the quark-antiquark luminosity. At SPS 7, where  $\tilde{m}_{\tilde{q}} \leq m_{\tilde{g}}$ , squarks are produced more copiously than gluinos, whereas the inverse is true at SPS 8. In both cases, the discovery reach extends to values of the effective SUSY-breaking scale  $\Lambda$  far above the actual benchmark points. It is clear that a striking monojet signal with large missing transverse energy could be discovered rapidly after the

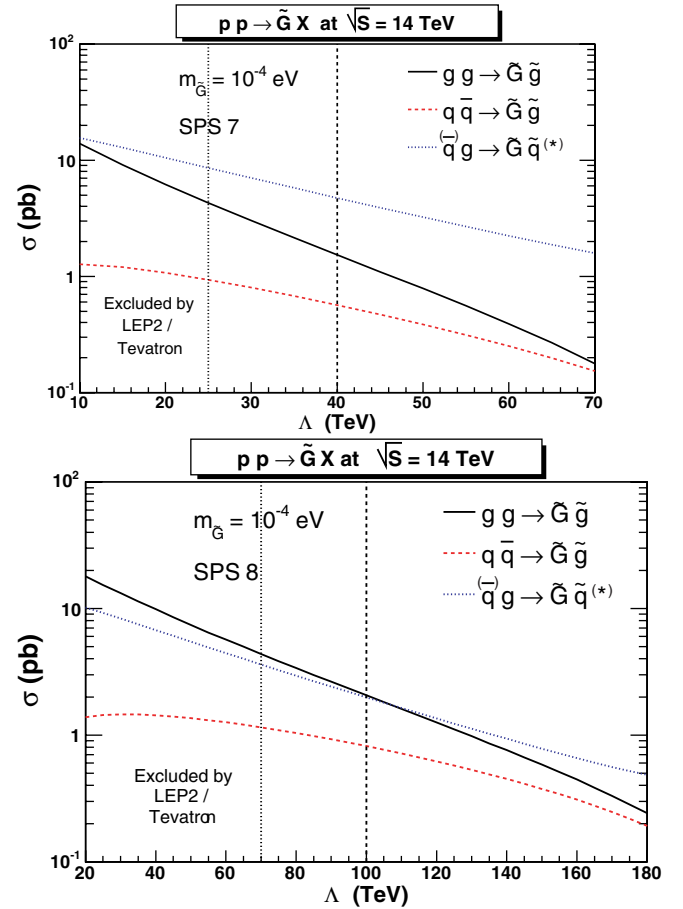


FIG. 11 (color online). Total cross sections of gravitino and gluino/squark associated production at the LHC for  $m_{\tilde{G}} = 10^{-4}$  eV and the GMSB benchmark slopes SPS 7 (top panel) and SPS 8 (bottom panel) as a function of the effective SUSY-breaking scale  $\Lambda$ .

startup of the LHC and with rather low luminosity. The only existing previous analysis for gravitino production at the LHC, based on the dominating subprocess  $gg \rightarrow \tilde{G} \tilde{g}$  only, assumed a slightly higher LHC center-of-mass energy of  $\sqrt{S} = 16$  TeV and fixed squark and gluino masses of 2 TeV and 750 GeV, respectively [9]. The authors computed a monojet cross section of similar size as the one shown in the lower part of Fig. 11 (8 pb for  $m_{\tilde{G}} = 10^{-4}$  eV) for comparable squark and gluino masses.

The transverse-momentum spectra at the LHC are shown in Fig. 12 for the two GMSB benchmark points and a gravitino mass of  $m_{\tilde{G}} = 10^{-4}$  eV. While the spectra peak again at values slightly below half of the squark/gluino masses, as was already the case at the Tevatron (see Fig. 9), they extend now to much larger values of  $p_T \approx 1200$  GeV. Note also that the absolute Tevatron cross section was only of similar size since it had been calculated with a smaller gravitino mass of  $m_{\tilde{G}} = 10^{-6}$  eV. In the high-luminosity phase at the LHC, the missing transverse-energy signal will be degraded by pileup events. In the

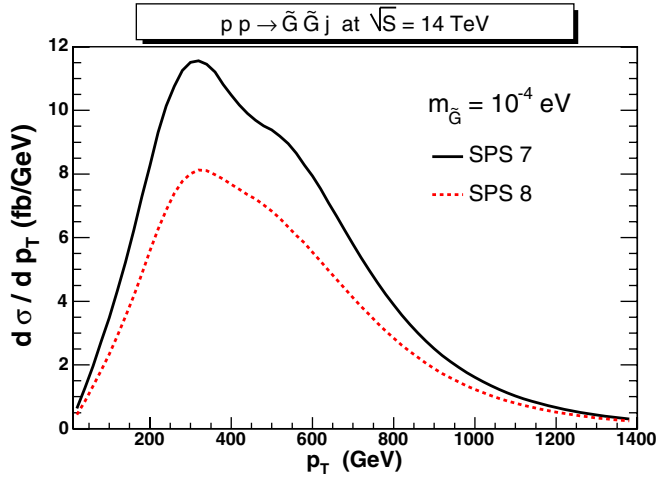


FIG. 12 (color online). Transverse-momentum spectra of the observed jet in gravitino production at the LHC for SPS 7 (solid line) and SPS 8 (dashed line).

ATLAS experiment, pileup can be eliminated and acceptable trigger rates in the kHz-range can be obtained for missing- $E_T$  thresholds of 60/120 GeV at low/high luminosity. These values can be 2 times lower if an additional hard jet of  $E_T > 100$  GeV is required [31]. As can be seen from Fig. 12, the signal cross section will be affected very little by these cuts.

#### IV. CONCLUSION

In this paper, we have derived the Feynman rules for light gravitino production and decay from an effective supergravity Lagrangian in four-component, nonderivative form and computed analytical partonic cross sections and branching ratios involving interactions of gravitinos, gluinos, and squarks. Special emphasis has been put on the gauge independence of the results, the contributions of quartic vertices, and a comparison with results obtained previously with a derivative Lagrangian and those obtained in the high-energy limit.

Using the narrow-width approximation, we combined the associated gravitino-squark/gluino production cross sections with the subsequent decay of the squarks/gluinos into quarks/gluons and a second gravitino. This enabled us to perform extensive numerical studies of branching ratios, of the total hadronic cross sections at the Tevatron and the LHC, and of the corresponding transverse-energy spectra of the single observed jet, then to impose experimental cuts on the latter, and finally to derive a new and robust exclusion contour in the  $m_{\tilde{G}}/m_{\tilde{q},\tilde{g}}$  plane from the latest CDF monojet cross section limit.

Our Tevatron exclusion contour implies that gravitinos with masses below  $2 \times 10^{-5}$  to  $1 \times 10^{-5}$  eV are excluded for squark/gluino masses below 200 and 500 GeV, respectively. These limits are complementary to the one obtained by the CDF Collaboration,  $1.1 \times 10^{-5}$  eV, under the assumption of very heavy squarks and gluinos.

For the LHC, we conclude that SUSY scenarios with light gravitinos, such as the GMSB benchmark slopes SPS 7 and 8, will lead to a striking monojet signal very quickly after its startup in 2008 and already with low luminosity. The missing- $E_T$  and jet trigger thresholds foreseen by the ATLAS Collaboration are perfectly suitable also in these scenarios for an efficient background reduction without affecting the signal in a significant way.

#### ACKNOWLEDGMENTS

M. K. gratefully acknowledges the hospitality of the Institute of Theoretical Physics at the University of Göttingen, where part of this work was completed.

#### APPENDIX A: EFFECTIVE LAGRANGIAN FOR SINGLE GOLDSTINOS

We start from the effective Lagrangian in four-component notation for the single interaction of a light gravitino [3,17,32,33], whose longitudinal (spin-1/2) goldstino components [2] can couple to the matter and gauge supermultiplets with enhanced (electroweak) strength [1]. The corresponding effective Lagrangian in two-component notation can be found in [14,34–40], while interactions involving several external goldstinos or goldstino propagators and the scalar/pseudoscalar superpartners of the goldstinos, the so-called sgoldstinos, have been derived in four-component notation, e.g., in [33,41].

By correctly translating the effective Lagrangian for light gravitinos in two-component notation [14,39] into the four-component notation of the traditional SUSY-QCD Lagrangian [42], we obtain the following nonderivative couplings for the interactions of Majorana-fermionic goldstinos  $\psi$  with Dirac-fermionic quarks  $\chi$ , complex-scalar squarks  $\phi$ , vector-bosonic gluons  $A_\mu^a$ , and Majorana-fermionic gluinos  $\lambda^a$ :

$$\begin{aligned} \mathcal{L}^{\text{eff}} = & \frac{m_q^2 - m_{\tilde{q}}^2}{\sqrt{3}Mm_{\tilde{G}}} (\bar{\chi} P_L \psi \phi_R - \bar{\chi} P_R \psi \phi_L + \bar{\psi} P_R \chi \phi_R^* \\ & - \bar{\psi} P_L \chi \phi_L^*) + \frac{im_{\tilde{g}}}{4\sqrt{6}Mm_{\tilde{G}}} \bar{\psi} [\gamma^\mu, \gamma^\nu] \lambda^a F_{\mu\nu}^a \\ & - \frac{g_s m_{\tilde{g}}}{\sqrt{6}Mm_{\tilde{G}}} \bar{\psi} \lambda^a \phi_i^* T_{ij}^a \phi_j. \end{aligned} \quad (\text{A1})$$

Here,  $M = (8\pi G_N)^{-1/2} = 2.435 \times 10^{18}$  GeV is the reduced Planck mass,  $m_{\tilde{G}}$  is the gravitino mass, which is related to the supersymmetry breaking vacuum expectation value  $\langle F \rangle$  in canonical normalization by  $m_{\tilde{G}} = \langle F \rangle / (\sqrt{3}M)$ , and  $g_s$  is the strong gauge coupling.  $T_{ij}^a$  are the generators of the  $SU(N_C = 3)$  color symmetry group with antisymmetric structure constants  $f^{abc}$  and Casimir operator  $C_F = 4/3$ , and  $P_{L,R} = (1 \mp \gamma_5)/2$  are the chirality projection operators. The squark and gluino masses will be denoted  $m_{\tilde{q}}$  and  $m_{\tilde{g}}$ . Since the top quark density in

hadrons is small, we can neglect the masses  $m_q$  of the five light quarks at high collision energies and consider the corresponding left- and right-handed squarks to be mass degenerate.

The effective theory contains the same couplings as the full theory [43,44], except for the quark-gluon-gravitino-squark vertex, which would violate the gauge symmetry in the effective theory [14], but was erroneously kept in the alternate Feynman rules of [12]. These were, however, not used there to calculate cross sections. In contrast, there is a new four-particle vertex [14,39], the gravitino-gluino-squark-squark vertex, which has been overlooked in all other cited references, but is neither relevant for our analysis nor for the one in [12]. Attention must also be paid to the assignment of factors of  $i$  in Eq. (A1), if the interference terms in [4,12] between scalar and gauge boson exchanges are to be correctly reproduced.

In the effective Lagrangian, all vertices are proportional to SUSY-breaking mass terms, i.e.  $m_{\tilde{q}}^2 - m_q^2$  and  $m_{\tilde{g}}$ . In particular, the Yukawa coupling of the goldstino can be obtained from that of the gluino by the replacement [3]

$$g_s T_{ij}^a \rightarrow \frac{m_{\tilde{q}}^2 - m_q^2}{\sqrt{6} M m_{\tilde{G}}}, \quad (\text{A2})$$

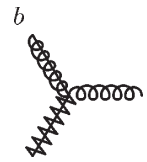
while the goldstino-gluon-gluino coupling can be obtained by the replacement

$$-g_s f^{abc} \gamma^\mu \rightarrow i \frac{m_{\tilde{g}}}{2\sqrt{6} M m_{\tilde{G}}} \delta^{ab} [\not{P}, \gamma^\mu] \quad (\text{A3})$$


with  $P$  representing the incoming gluon-momentum. At high energies, contributions involving the cubic goldstino-quark-squark coupling are suppressed relative to the gluino contribution due to the higher mass dimension of the coupling.

## APPENDIX B: FEYNMAN RULES FOR SINGLE GOLDSTINOS

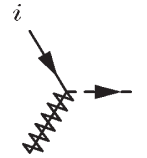
In order to derive the Feynman rules needed for the hadronic production and decay of single goldstinis, we multiply the effective Lagrangian in Eq. (A1) with a factor of  $i$ , perform a Fourier transformation, and take the functional derivative with respect to the external fields. Denoting the incoming four-momentum by  $P$ , the chirality projection operators by  $P_{L,R} = (1 \mp \gamma_5)/2$ , Lorentz indices by  $\mu, \nu, \dots$ , and color indices of the fundamental (adjoint) representation of the color symmetry group SU(3) by  $i, j, \dots (a, b, \dots)$ , we obtain the following interaction vertices:



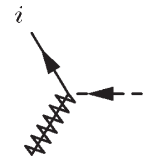
$$P, a, \mu + i \frac{m_{\tilde{g}}}{2\sqrt{6} M m_{\tilde{G}}} \delta^{ab} [\not{P}, \gamma^\mu]. \quad (\text{B1})$$



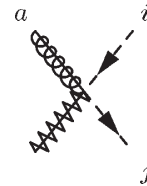
$$+ \frac{m_{\tilde{g}}}{2\sqrt{6} M m_{\tilde{G}}} g_s f^{abc} [\gamma^\mu, \gamma^\nu]. \quad (\text{B2})$$



$$j \mp i \frac{m_{\tilde{q}}^2 - m_q^2}{\sqrt{3} M m_{\tilde{G}}} \delta_{ij} P_{L,R}. \quad (\text{B3})$$



$$-j \mp i \frac{m_{\tilde{q}}^2 - m_q^2}{\sqrt{3} M m_{\tilde{G}}} \delta_{ij} P_{R,L}. \quad (\text{B4})$$



$$-i \frac{m_{\tilde{g}}}{\sqrt{6} M m_{\tilde{G}}} g_s T_{ij}^a. \quad (\text{B5})$$

Here, the arrows on (s)quark lines indicate flavor flow, while the Majorana nature of gravitinos and gluinos requires the fermion flow to be fixed arbitrarily [45]. These Feynman rules have been implemented into the computer algebra program FEYNARTS [46,47], and the corresponding model file is available from the authors upon request. The derivative forms of the (s)goldstino interaction vertices in two-component form were already implemented some time ago into the program COMPHEP [48].

Our Feynman rules differ from those presented in Appendix A.3.3 of [49], which have also been derived from [14], by a factor of  $i$  in the first two vertices, apparently due to a misinterpretation of the two-component tensor  $\sigma^{\mu\nu}$  [50]. The Feynman rules in [51] differ from ours in addition by an irrelevant global factor of  $i$ . The usual SUSY-QCD vertices and propagators can be found, e.g., in [52].

- [1] P. Fayet, Phys. Lett. **70B**, 461 (1977).
- [2] R. Casalbuoni, S. De Curtis, D. Dominici, F. Feruglio, and R. Gatto, Phys. Lett. B **215**, 313 (1988).
- [3] P. Fayet, Phys. Lett. B **175**, 471 (1986).
- [4] J. L. Lopez, D. V. Nanopoulos, and A. Zichichi, Phys. Rev. D **55**, 5813 (1997).
- [5] F. Abe *et al.* (CDF Collaboration), Phys. Rev. Lett. **62**, 1825 (1989).
- [6] D. A. Dicus, S. Nandi, and J. Woodside, Phys. Rev. D **41**, 2347 (1990).
- [7] F. Abe *et al.* (CDF Collaboration), Phys. Rev. Lett. **76**, 2006 (1996).
- [8] D. A. Dicus and S. Nandi, Phys. Rev. D **56**, 4166 (1997).
- [9] M. Drees and J. Woodside, Report No. IS-J-4137 and No. CERN 90-10.
- [10] M. Viel, J. Lesgourgues, M. G. Haehnelt, S. Matarrese, and A. Riotto, Phys. Rev. D **71**, 063534 (2005).
- [11] W. Beenakker, R. Höpker, M. Spira, and P. M. Zerwas, Nucl. Phys. **B492**, 51 (1997).
- [12] J. Kim, J. L. Lopez, D. V. Nanopoulos, R. Rangarajan, and A. Zichichi, Phys. Rev. D **57**, 373 (1998).
- [13] M. Bolz, A. Brandenburg, and W. Buchmüller, Nucl. Phys. **B606**, 518 (2001).
- [14] T. Lee and G. H. Wu, Phys. Lett. B **447**, 83 (1999).
- [15] S. Ambrosiano, G. L. Kane, G. D. Kribs, S. P. Martin, and S. Mrenna, Phys. Rev. D **54**, 5395 (1996).
- [16] S. P. Martin, arXiv:hep-ph/9709356.
- [17] G. F. Giudice and R. Rattazzi, Phys. Rep. **322**, 419 (1999).
- [18] B. C. Allanach *et al.*, Eur. Phys. J. C **25**, 113 (2002).
- [19] W. M. Yao *et al.* (Particle Data Group), J. Phys. G **33**, 1 (2006).
- [20] A. Djouadi, J. L. Kneur, and G. Moultaka, Comput. Phys. Commun. **176**, 426 (2007).
- [21] M. Mühlleitner, A. Djouadi, and Y. Mambrini, Comput. Phys. Commun. **168**, 46 (2005). This program includes the branching ratios for a neutralino NLSP into gravitinos,  $\tilde{\chi}_1^0 \rightarrow \tilde{G}\gamma$ ,  $\tilde{\chi}_1^0 \rightarrow \tilde{G}Z^0$ , and  $\tilde{\chi}_1^0 \rightarrow \tilde{G}h^0$ , as well as the one for a light stau NLSP,  $\tilde{\tau}_1 \rightarrow \tilde{G}\tau$ , but not those for gluinos and squarks.
- [22] R. Rangarajan (private communication).
- [23] J. Pumplin, D. R. Stump, J. Huston, H. L. Lai, P. Nadolsky, and W. K. Tung, J. High Energy Phys. 07 (2002) 012.
- [24] V. Shiltsev, Fermilab Report No. FERMILAB-CONF-04-123-AD, 2004 (unpublished).
- [25] A. A. Affolder *et al.* (CDF Collaboration), Phys. Rev. Lett. **85**, 1378 (2000).
- [26] A. Brignole, F. Feruglio, M. L. Mangano, and F. Zwirner, Nucl. Phys. **B526**, 136 (1998); **B582**, 759(E) (2000).
- [27] A. Castro (private communication).
- [28] T. Bhattacharya and P. Roy, Nucl. Phys. **B328**, 469 (1989).
- [29] V. M. Abazov *et al.* (D0 Collaboration), Phys. Rev. Lett. **90**, 251802 (2003).
- [30] A. Abulencia *et al.* (CDF Collaboration), Phys. Rev. Lett. **97**, 171802 (2006).
- [31] R. S. Dubitzky, K. Jakobs, E. Bagheri, K. Mahboubi, and M. Wunsch, Report No. ATL-DAQ-99-011 and No. HD-IHEP-98-05.
- [32] T. Moroi, H. Murayama, and M. Yamaguchi, Phys. Lett. B **303**, 289 (1993).
- [33] T. Gherghetta, Nucl. Phys. **B485**, 25 (1997).
- [34] T. E. Clark and S. T. Love, Phys. Rev. D **54**, 5723 (1996).
- [35] A. Brignole, F. Feruglio, and F. Zwirner, Nucl. Phys. **B501**, 332 (1997).
- [36] A. Brignole, F. Feruglio, and F. Zwirner, J. High Energy Phys. 11 (1997) 001.
- [37] M. A. Luty and E. Ponton, Phys. Rev. D **57**, 4167 (1998).
- [38] T. E. Clark, T. Lee, S. T. Love, and G. H. Wu, Phys. Rev. D **57**, 5912 (1998).
- [39] T. Lee and G. H. Wu, Mod. Phys. Lett. A **13**, 2999 (1998).
- [40] A. Brignole, E. Perazzi, and F. Zwirner, J. High Energy Phys. 09 (1999) 002.
- [41] A. Brignole, F. Feruglio, and F. Zwirner, Nucl. Phys. **B516**, 13 (1998); **B555**, 653(E) (1999).
- [42] H. E. Haber and G. L. Kane, Phys. Rep. **117**, 75 (1985).
- [43] E. Cremmer, S. Ferrara, L. Girardello, and A. Van Proeyen, Nucl. Phys. **B212**, 413 (1983).
- [44] J. Wess and J. Bagger, *Supersymmetry and Supergravity* (Princeton University Press, Princeton, 1992), 2nd ed.
- [45] A. Denner, H. Eck, O. Hahn, and J. Küblbeck, Nucl. Phys. **B387**, 467 (1992).
- [46] J. Küblbeck, M. Böhm, and A. Denner, Comput. Phys. Commun. **60**, 165 (1990).
- [47] T. Hahn and C. Schappacher, Comput. Phys. Commun. **143**, 54 (2002).
- [48] D. S. Gorbunov and A. V. Semenov, arXiv:hep-ph/0111291.
- [49] M. Bolz, Report No. DESY-THESIS-2000-013 (unpublished).
- [50] T. Lee (private communication).
- [51] T. Moroi, Ph.D. thesis, Tohoku University, Report No. TU-479 [arXiv:hep-ph/9503210].
- [52] R. Höpker, Report No. DESY-T-96-02 (unpublished).